On the phase noise performance of microwave and millimeter-wave signals generated with versatile Kerr optical frequency combs

KHALDOUN SALEH[1,2] AND YANNE K. CHEMBO[1,*]

[1]*FEMTO-ST Institute [CNRS UMR6174], Optics Department, Univ. Bourgogne Franche-Comté, 15B Avenue des Montboucons, 25030 Besançon cedex, France*
[2]*Currently with the FEMTO-ST Institute [CNRS UMR6174], Time-Frequency Department, Univ. Bourgogne Franche-Comté, 26 Chemin de l'Epitaphe, 25030 Besançon cedex, France*
[*]*yanne.chembo@femto-st.fr*

Abstract: We investigate the phase noise performance of micro- and millimeter-wave signals generated using a ultra-high Q whispering gallery mode disk-resonator with Kerr nonlinearity. Our study focuses on the stability of the optical spectra and on the performances of the corresponding microwave and millimeter-wave beat notes in terms of power and phase noise. The blue slope of an optical mode of the resonator, allowing for the generation of optical frequency combs, is accurately explored in order to identify various comb patterns. Each of these patterns is characterized in the optical and radio-frequency domains. Phase noise levels below -100 dBc/Hz at 10 kHz offset have been achieved for beat notes in the radio-frequency spectrum at 12 GHz, 18 GHz, 24 GHz, 30 GHz, and 36 GHz with the same resonator.

References and links

1. A. B. Matsko and V. S. Ilchenko, "Optical resonators with whispering gallery modes I: Basics," IEEE J. Sel. Top. Quantum Electron. **12**, 3 (2006).
2. V. S. Ilchenko and A. B. Matsko, "Optical resonators with whispering-gallery modes–part II: applications," IEEE J. Sel. Top. Quantum Electron. **12**, 15 (2006).
3. A. Chiasera, Y. Dumeige, P. Feron, M. Ferrari, Y. Jestin, G. Nunzi Conti, S. Pelli, S. Soria, and G. C. Righini, "Spherical whispering-gallery-mode microresonators," Laser Photonics Rev. **4**, 457–482 (2010).
4. A. A. Savchenkov, A. B. Matsko, V. S. Ilchenko, and L. Maleki, "Optical resonators with ten million finesse," Opt. Express **115**, 6768 (2007).
5. L. Maleki, "The optoelectronic oscillator," Nat. Photonics **5**, 728 (2011).
6. S. B. Papp, P. Del'Haye, and S. A. Diddams, "Mechanical control of a microrod-resonator optical frequency comb," Phys. Rev. X. **3**, 031003 (2013).
7. G. Lin, S. Diallo, R. Henriet, M. Jacquot, and Y. K. Chembo, "Barium fluoride whispering-gallery-mode disk-resonator with one billion quality-factor," Opt. Lett. **39**, 6009–6012 (2014).
8. R. Henriet, G. Lin, A. Coillet, M. Jacquot, L. Furfaro, L. Larger, and Y. K. Chembo, "Kerr optical frequency comb generation in strontium fluoride whispering-gallery mode resonators with billion quality factor," Opt. Lett. **40**, 1567–1570 (2015).
9. T. J. Kippenberg, S. M. Spillane, and K. J. Vahala, "Kerr-nonlinearity optical parametric oscillation in an ultrahigh-Q toroid microcavity," Phys. Rev. Lett. **93**, 083904 (2004).
10. A. A. Savchenkov , A. B. Matsko, D. Strekalov, M. Mohageg, V. S. Ilchenko, and L. Maleki, "Low threshold optical oscillations in a whispering gallery mode CaF_2 resonator," Phys. Rev. Lett. **93**, 243905 (2004).
11. P. Del'Haye, A. Schliesser, O. Arcizet, T. Wilken, R. Holzwarth, and T. J. Kippenberg, "Optical frequency comb generation from a monolithic microresonator," Nature **450**, 1214–1217 (2007).
12. Y. K. Chembo and N. Yu, "Modal expansion approach to optical-frequency-comb generation with monolithic whispering-gallery-mode resonators," Phys. Rev. A **82**, 033801 (2010).
13. A. B. Matsko, A. A. Savchenkov, and L. Maleki, "Normal group-velocity dispersion Kerr frequency comb," Opt. Lett. **37**, 43 (2012).
14. A. B. Matsko, A. A Savchenkov, W. Liang, V. S. Ilchenko, D. Seidel, and L. Maleki, "Mode-locked Kerr frequency combs," Opt. Lett. **36**, 2845 (2011).
15. Y. K. Chembo and C. R. Menyuk, "Spatiotemporal Lugiato-Lefever formalism for Kerr-comb generation in whispering-gallery mode resonators," Phys. Rev. A **87**, 053852 (2013).

16. S. Coen, H. G. Randle, T. Sylvestre and M. Erkintalo, "Modeling of octave-spanning Kerr frequency combs using a generalized mean-field Lugiato-Lefever model," Opt. Lett. **38**, 37 (2013).

17. A. Coillet I. Balakireva, R. Henriet, K. Saleh, L. Larger, J. M. Dudley, C. R. Menyuk, and Y. K. Chembo, "Azimuthal turing patterns, bright and dark cavity solitons in Kerr combs generated with whispering-gallery-mode resonators," IEEE Photonics J. **5**, 6100409 (2013).

18. L. A. Lugiato and R. Lefever, "Spatial dissipative structures in passive optical systems," Phys. Rev. Lett. **58**, 2209 (1987).

19. C. Godey, I. V. Balakireva, A. Coillet, and Y. K. Chembo, "Stability analysis of the spatiotemporal Lugiato-Lefever model for Kerr optical frequency combs in the anomalous and normal dispersion regimes," Phys. Rev. A **89**, 063814 (2014).

20. P. Parra-Rivas, D. Gomila, M. A. Matias, S. Coen, and L. Gelens, "Dynamics of localized and patterned structures in the Lugiato-Lefever equation determine the stability and shape of optical frequency combs," Phys. Rev. A. **89**, 043813 (2014).

21. T. J. Kippenberg, R. Holzwarth, and S. A. Diddams, "Microresonator-based optical frequency combs," Science **332**, 555-559 (2011).

22. Y. K. Chembo, "Kerr optical frequency combs: theory, applications and perspectives," Nanophotonics **5**, 214–230 (2016).

23. T. Herr, K. Hartinger, J. Riemensberger, C. Y. Wang, E. Gavartin, R. Holzwarth, M. L. Gorodetsky, and T. J. Kippenberg, "Universal formation dynamics and noise of Kerr-frequency combs in microresonators," Nat. Photonics **6**, 480–487 (2012).

24. A. Savchenkov, A. Matsko, and L. Maleki, "On frequency combs in monolithic resonators", Nanophotonics **5**, 363–391 (2016).

25. T. Herr, V. Brasch, J. D. Jost, C. Y. Wang, N. M. Kondratiev, M. L. Gorodetsky, and T. J. Kippenberg, "Temporal solitons in optical microresonators," Nat. Photonics **8**, 145–152 (2014).

26. P.-H. Wang, F. Ferdous, H. Miao, J. Wang, D. E. Leaird, K. Srinivasan, L. Chen, V. Aksyuk, and A. M. Weiner, "Observation of correlation between route to formation, coherence, noise, and communication performance of Kerr combs," Opt. Express **20** 29284–29295 (2012).

27. J. Levy, K. Saha, Y. Okawachi, M. Foster, A. Gaeta, and M. Lipson, "High-performance silicon-nitride-based multiple-wavelength source," IEEE Photonics Technol. Lett. **24**, 1375 (2012).

28. J. Pfeifle, V. Brasch, M. Lauermann, Y. Yu, D. Wegner, T. Herr, K. Hartinger, P. Schindler, J. Li, D. Hillerkuss, R. Schmogrow, C. Weimann, R. Holzwarth, W. Freude, J. Leuthold, T. J. Kippenberg, and C. Koos, "Coherent terabit communications with microresonator Kerr frequency combs," Nat. Photonics **8**, 375–380 (2014).

29. J. Pfeifle, A. Coillet, R. Henriet, K. Saleh, P. Schindler, C. Weimann, W. Freude, I. V. Balakireva, L. Larger, C. Koos, and Y. K. Chembo, "Optimally coherent Kerr combs generated with crystalline whispering gallery mode resonators for ultrahigh capacity fiber communications," Phys. Rev. Lett. **114** 093902 (2015).

30. C. Y. Wang, T. Herr, P. Del'Haye, A. Schliesser, J. Hofer, R. Holzwarth, T. W. Hansch, N. Picqué, and T. J. Kippenberg, "Mid-infrared optical frequency combs at 2.5 μm based on crystalline microresonators," Nat. Commun. **4**, 1345 (2012).

31. A. A. Savchenkov, V. S. Ilchenko, F. Di Teodoro, P. M. Belden, W. T. Lotshaw, A. B. Matsko, and L. Maleki, "Generation of Kerr combs centered at 4.5 μm in crystalline microresonators pumped with quantum-cascade lasers," Opt. Lett. **40**, 3468–3471 (2015).

32. J. Li, H. Lee, T. Chen, and K. J. Vahala, "Low-pump-power, low-phase-noise, and microwave to millimeter-wave repetition rate operation in microcombs," Phys. Rev. Lett. **109** 233901 (2012).

33. A. A. Savchenkov, D. Eliyahu, W. Liang, V. S. Ilchenko, J. Byrd, A. B. Matsko, D. Seidel, and L. Maleki, "Stabilization of a Kerr frequency comb oscillator," Opt. Lett. **38**, 2636–2639 (2013)

34. P. Del'Haye, S. B. Papp, and S. A. Diddams, "Hybrid electro-optically modulated microcombs," Phys. Rev. Lett. **109** 263901 (2012).

35. S. B. Papp, K. Beha, P. Del'Haye, F. Quinlan, H. Lee, K. J. Vahala, and S. A. Diddams, "Microresonator frequency comb optical clock," Optica **1**, 10–14 (2014).

36. A. B. Matsko and L. Maleki, "Noise conversion in Kerr comb RF photonic oscillators," J. Opt. Soc. Am. B **32**, 232–240 (2015).

37. W. Liang, D. Eliyahu, V. S. Ilchenko, A. A. Savchenkov, A. B. Matsko, D. Seidel, L. Maleki, "High spectral purity Kerr frequency comb radio frequency photonic oscillator," Nat. Commun. **6**, 7957 (2015).

38. G. Lin, K. Saleh, R. Henriet, S. Diallo, R. Martinenghi, A. Coillet, and Y. K. Chembo, "Wide-range tunability, thermal locking, and mode-crossing effects in Kerr optical frequency combs," Opt. Eng. **53**, 122602 (2014).

39. G. Lin, R. Martinenghi, S. Diallo, K. Saleh, A. Coillet, and Y. K. Chembo, "Spectro-temporal dynamics of Kerr combs with parametric seeding," Appl. Opt. **54**, 2407-2412 (2015).

40. A. Coillet, R. Henriet, K. P. Huy, M. Jacquot, L. Furfaro, I. Balakireva, L. Larger, and Y. K. Chembo, "Microwave photonics systems based on whispering-gallery-mode resonators," J. Vis. Exp. **78**, e50423 (2013).

41. K. Saleh, R. Henriet, S. Diallo, G. Lin, R. Martinenghi, I. V. Balakireva, P. Salzenstein, A. Coillet, and Y. K. Chembo, "Phase noise performance comparison between optoelectronic oscillators based on optical delay lines and whispering gallery mode resonators,". Opt. Express **22**, 32158–32173 (2014).

42. Y. Dumeige, S. Trebaol, L. Ghisa, T. K. N. Nguyen, H. Tavernier, and P. Feron, "Determination of coupling pattern

of high-Q resonators and optical gain of highly selective amplifiers," J. Opt. Soc. Am. B **25**, 2073–2080 (2008).
43. T. Carmon, L. Yang, and K. Vahala, "Dynamical thermal behavior and thermal self-stability of microcavities," Opt. Express **12**, 4742–4750 (2004).
44. P. Del'Haye, A. Coillet, W. Loh, K. Beha, S. B. Papp, and S. A. Diddams, "Phase steps and resonator detuning measurements in microresonator frequency combs," Nat. Commun. **6**, 5668 (2015).
45. A. Coillet and Y. K. Chembo, "On the robustness of phase-locking in Kerr optical frequency combs," Opt. Lett. **39**, 1529 (2014).
46. G. Lin and Y. K. Chembo, "On the dispersion management of fluorite whispering-gallery mode resonators for Kerr optical frequency comb generation in the telecom and mid-infrared range," Opt. Express **23**, 1594-1604 (2015).
47. I. S. Grudinin and N. Yu, "Dispersion engineering of crystalline resonators via microstructuring," Optica **2**, 221–224 (2015).
48. A. Coillet and Y. K. Chembo, "Routes to spatiotemporal chaos in Kerr optical frequency combs," Chaos **24**, 013313 (2014).
49. A. Coillet, J. Dudley, G. Genty, L. Larger, and Y. K. Chembo "Optical rogue waves in whispering-gallery-mode resonators," Phys. Rev. A **89**, 013835 (2014).
50. A. B. Matsko, A. A. Savchenkov, N. Yu, and L. Maleki, "Whispering-gallery-mode resonators as frequency references. I. Fundamental limitations," J. Opt. Soc. Am. B **24**, 1324 (2007).
51. A. A. Savchenkov, A. B. Matsko, V. S. Ilchenko, N. Yu, and L. Maleki, "Whispering-gallery-mode resonators as frequency references. II. Stabilization," J. Opt. Soc. Am. B **24**, 2988 (2007).
52. K. Saleh, G. Lin and Y. K. Chembo, "Effect of laser coupling and active stabilization on the phase noise performance of optoelectronic microwave oscillators based on whispering-gallery-mode resonators," IEEE Photonics J. **7**, 1-11 (2015).
53. K. Saleh, O. Llopis, and G. Cibiel, "Optical scattering induced noise in fiber ring resonators and optoelectronic oscillators," IEEE J. Lightwave Technol. **31**, 1433–1446 (2013).
54. G. Lin, S. Diallo, K. Saleh, R. Martinenghi, J.-C. Beugnot, T. Sylvestre, and Y. K. Chembo, "Cascaded Brillouin lasing in monolithic barium fluoride whispering gallery mode resonators," Appl. Phys. Lett. **105**, 231103 (2014).

1. Introduction

High stability and spectral purity microwave and millimeter-wave sources have become increasingly crucial in several areas of applications, including communication systems, signal processing, radars, radio astronomy, satellites, GPS navigation, spectroscopy, time-frequency metrology, etc. Although highly efficient, best microwave sources currently suffer from numerous shortcomings. Most of them are bulky, complex, non-tunable, non-transportable and they also feature very limited performances as long as the application frequency increases (e.g. frequency multiplied quartz oscillators).

For more than twenty years, optics has started to prove itself as an elegant and reliable solution for the development of microwave and even millimeter-wave sources featuring very high spectral purity. The advent of optical frequency combs generated by femtosecond lasers in the late 1990s has revolutionized the measurement of time and frequency. These lasers have allowed the establishment of a "bridge" linking both ends of the electromagnetic spectrum between them. Following this discovery, the principle of optical frequency division of an ultra-pure laser to much lower frequencies (microwave frequency range), using an optical frequency comb featuring a mode spacing of few hundreds of MHz, has been demonstrated, but unfortunately, it remains at this date exclusively a laboratory technology.

A novel method to generate ultra-pure microwaves is based on using ultra-high Q whispering gallery mode resonators (WGMRs). These resonators can trap photons in their eigenmodes by total internal reflections and are core elements in a wide variety of photonics applications (see review articles [1–3]). Some of these resonators can feature a Q factor as high as 10^{11} at 1550 nm [4]. They can be integrated in compact setups [5] and even mass-produced [6]. In most applications related to ultra-pure microwave generation, the WGM cavities are mm-size disk-resonators with $Q \sim 10^9$ at 1550 nm [7, 8], and they feature a free-spectral range of the order of 10 GHz, suitable for aerospace and telecom applications.

Owing to the strong confinement of pump photons and to their long lifetime, nonlinear effect such as the Kerr interaction are enhanced in the resonator. As a consequence, above a certain threshold, the pump photons undergo a frequency shift and populate the neighboring eigenmodes

of the WGMR, thereby creating the so-called Kerr optical frequency comb. Pioneering works on this type of hyper-parametric interaction were reported in refs. [9–11]. The theoretical understanding of this phenomenon can be achieved either using a modal expansion model [12,13] or a spatiotemporal model [14–17] based on the Lugiato-Lefever equation [18]. The theoretical analysis of Kerr comb generation has shown that the intracavity field can morph into many types of dissipative structures, including solitons, roll patterns, breathers, and even spatiotemporal chaos [19, 20]. Comprehensive reviews on the topic of Kerr comb generation and applications can be found in refs. [21, 22].

Several studies are particularly focused on the understanding and the beneficial use of these Kerr optical frequency combs, generated with high quality factors WGMRs [23, 24]. They are motivated by the important gain that Kerr combs could provide in terms of compactness, low power consumption and high frequency generation, in various fields of applications: generation of femtosecond pulses [25], in telecommunications [26–29], spectroscopy [30, 31], etc. Once completely understood and controlled, a Kerr comb could particularly replace the bulky and power consuming femtosecond laser in an optical frequency division based generator. This will consequently make possible the generation of ultra-pure microwave, millimeter wave and even sub-millimeter-wave signals in a compact and low consumption generator, further revolutionizing the measurement of time and frequency [32–37].

In this article, we present several experimental investigations performed on optical Kerr combs generated in a crystalline three-dimensional disk-shaped WGMR made of magnesium fluoride (MgF_2) and featuring a high optical quality factor (Q_{opt}). These studies are in the continuity of our previous theoretical and experimental investigations performed on Kerr combs, and aiming the understanding of their complex dynamics and later their beneficial use [17, 38, 39]. We first describe the MgF_2 WGMR used in this work and its characteristics, and the principle of Kerr combs generated in this WGMR. After the identification of a useful optical mode of the WGMR, allowing the generation of Kerr combs, we present the followed procedure to stabilize the laser lightwave on the edge of the blue slope of this optical mode. This allows us later on to accurately investigate the mode blue slope and to identify six different generated Kerr comb patterns. These patterns are then accurately characterized in the optical and radio frequency domains, and the performances of the corresponding microwave and millimeter-wave beat notes are evaluated in terms of RF power and phase noise. All the measured optical, RF and phase noise spectra of the various signals are presented and discussed.

2. Kerr comb generation

The MgF_2 WGMR, having a 12 mm in diameter and that we used in this work, was fabricated in our laboratory [40] [see Fig. 1(a)]. The 12 mm here is the raw disk diameter before the fabrication process, which consists in grinding and polishing. The WGMR free spectral range (FSR) mainly depends on its geometry and particularly on its circumference, since the resonant lightwave orbits just beneath the surface in such structures. This free spectral range can be determined as FSR $= c/\pi n_g d$, where c is the speed of light, d is the diameter of the WGMR and n_g is the material's group veleocity dispersion index of the MgF_2 disk ($n_g = 1.37$ at a wavelength $\lambda = 1548$ nm). Assuming a perfectly circular MgF_2 disk with 12 mm diameter, the FSR of its fundamental mode family should be equal to 5.8 GHz. In reality, this FSR value will be slightly higher, as one should take into account the fact that the WGMR diameter becomes slightly less than 12 mm after all the fabrication steps.

To be able to use this WGMR, the laser lightwave, generated by a Koheras fiber laser with sub-kHz linewidth, was first coupled into the WGMR. This was achieved using a homemade tapered optical microfiber in an add-only configuration [and later in an add-drop coupling configuration; see Fig. 2(a)], enabling the WGMs to be efficiently excited in the WGMR. The tapered optical microfibers we used in our experiments typically had less than 0.22 dB transmission loss and their
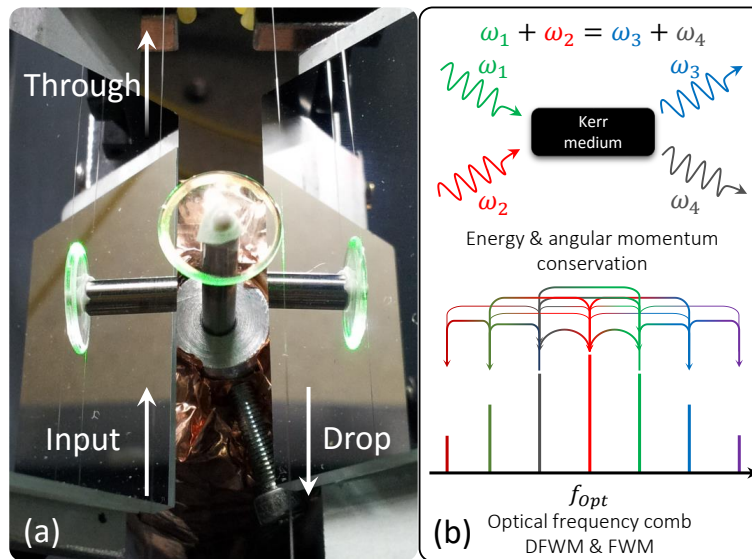
Fig. 1. (a) MgF_2 WGMR fixed on a specific mount and coupled to (one or two) tapered optical microfibers. Two mirrors facing each other are used to get an accurate side view of the microfibers position regarding the WGMR rim. (b) Illustration of (Degenerate) Four-Wave-Mixing [(D)FWM] for Kerr comb generation.

tapered part was usually few millimeters long with a 1 μm waist diameter. They were clamped on nanometric xyz translation stages. The laser-WGMR coupling was therefore controlled with high precision. After the establishment of an add-only coupling, the WGMR was characterized in the optical domain using two techniques: the laser wavelength scanning technique and the cavity-ring-down (CRD) technique [41]. The first one consists of a frequency fine-tuning of the laser frequency and allows a good visualization of the WGMR different optical mode families by recording the WGMR response on a photodiode followed by an oscilloscope [see Fig. 2(c)]. Figure 3 presents the normalized absorption signal recorded at the photodiode output by an oscilloscope and it shows different optical modes exited in the WGMR. Moreover, using this characterization technique, we can also get an estimation of the FSRs of some optical mode families [41]. The CRD technique is the same as for the laser wavelength scanning technique, except the laser frequency is rapidly tuned in this case. It consists of measuring the photon lifetime τ_p inside the resonant cavity by studying its relaxation pattern, giving access to its intrinsic quality factor (Q_{opt-i}) [42].

The inset figure in Fig. 3 presents the normalized absorption signal of the useful optical mode that has been identified amongst different eigenmodes of the WGMR. This mode was indeed able to support the generation of several Kerr comb patterns in the optical mode blue side, as we will see later. Using the aforementioned characterization techniques (with low optical power scanning laser), we have been able to measure a 6.1 GHz FSR for identified optical mode family and a Q_{opt-i} of 6×10^8. Thanks to relatively optimized lightwave coupling, a FWHM of 1.2 MHz has been measured and therefore a WGMR loaded Q_{opt} of 1.6×10^8 can be calculated.

Here it is noteworthy to mention the visible optical mode broadening in the inset figure in Fig. 3. This broadening was due to the high power of the gradually resonant laser lightwave in the MgF_2 WGMR needed to generate the Kerr combs. In reality, while the laser is scanning the optical mode from its blue side towards its red side, a heat is generated, causing a thermal red shift in the optical mode in the same direction of the scanning laser. This consequently broadens
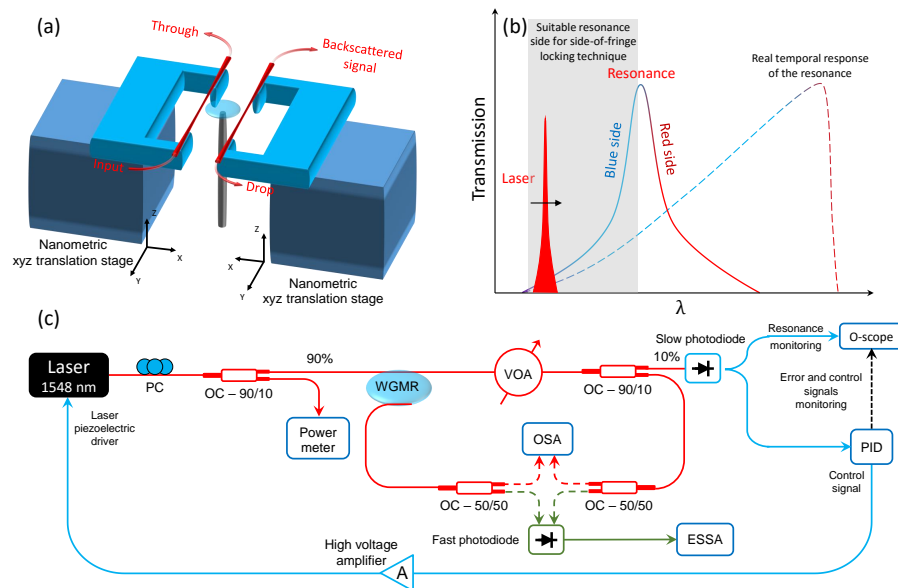
Fig. 2. (a) Optical coupling bench using one (two) nanometric xyz translation stage(s) for add-only (add-drop) coupling configuration. (b) Illustration showing the resonance blue-slope that could be probed by the laser lightwave in a MgF_2 WGMR, imprecisely using the thermal locking technique and accurately using the side-of-fringe locking technique. An illustration of the real temporal response of the resonance (resonance thermal shift and broadening), obtained when the laser is scanning the resonance from its blue slope to the red slope, is also given. (c) Experimental setup, including the side-of-fringe laser locking loop, used to probe the different Kerr comb patterns generated in the MgF_2 WGMR. In red: optical path; In green: RF path; In blue: low frequency path for the locking loop; PC: polarization controller; VOA: variable optical attenuator; OC: optical fiber coupler; O-scope: oscilloscope; PID: proportional-integral-derivative controller; OSA: optical spectrum analyzer; ESSA: electrical signal and spectrum analyzer.

the visualized optical mode [see the illustration in Fig. 2(b)]. In MgF_2 WGMR, this phenomenon can be useful to passively lock the laser lightwave on the blue slope of the optical mode. This can be done when a thermal equilibrium is established between the injected optical power of the gradually resonant laser lightwave and the thermal drift of the optical mode [43]. On the other hand, the laser-mode locking state (point) cannot be accurately controlled using this technique.

In a Kerr-nonlinear optical resonator like the MgF_2 WGMR, a laser lightwave coupled to an optical mode of the resonator can give rise to two new lightwaves above a certain threshold depending on the resonator Q_{opt}, mode volume, material and geometric dispersion, nonlinearity, etc. The new lightwaves will be spaced by a multiple of the FSR of the resonator on either side of the laser lightwave. At the end, a large number of modes of the resonator will be populated thanks to the Kerr effect [by FWM and DFWM; see the illustration in Fig. 1(b)]. The different lightwaves (comb teeth) generated around the laser lightwave will thus form together what we call a Kerr optical frequency comb. In this comb, all generated lightwaves will have linewidths equivalent to that of the laser and the frequency fluctuations of all components of the Kerr comb will be correlated, under the condition of a coherent regime of the Kerr comb [23, 37, 44]. Consequently, the beat of the Kerr comb on a fast photodiode will generate RF signals with frequencies equal to the FSR of the Kerr comb (FSR_C: spacing between the comb teeth) and to its harmonics,
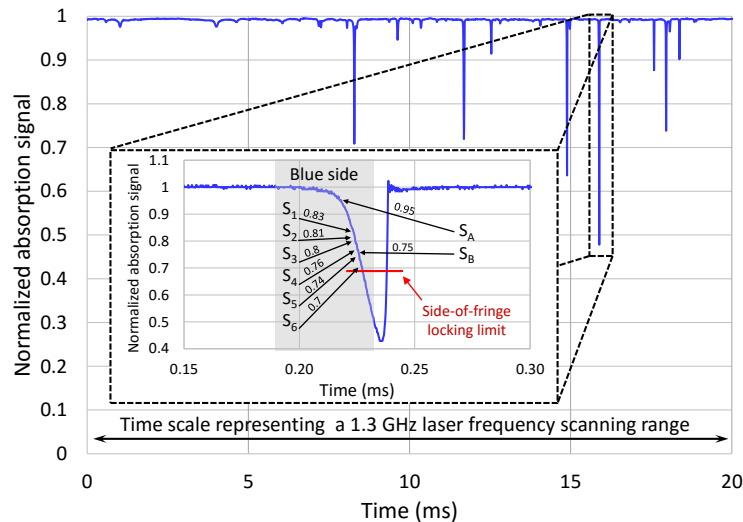
Fig. 3. Normalized absorption signal recorded at the slow photodiode output by an oscilloscope for the MgF$_2$ WGMR, where different excited optical modes can be seen. The 20 ms time scale on this graphic represents a 1.3 GHz laser frequency scanning range (visualization window). The inset figure shows the WGMR mode that has been used in our experiment and accurately investigated using the side-of-fringe locking technique in order to identify the different generated Kerr comb patterns. The various laser-mode locking states that has been considered are also shown (S$_1$, S$_2$, etc.). The red line draws the locking limit imposed by the laser frequency noise combined to the WGMR thermal instabilities, and also to the limits of the side-of-fringe locking scheme.

and featuring linewidths several orders of magnitude narrower than that of the laser [37]. The properties of the comb therefore mainly depend on the pumping laser characteristics, as well as on the resonator shape, size and material, and on the lightwave coupling configuration and the setup isolation [24].

3. Characterizing the Kerr comb patterns

Kerr combs have very complex dynamics with different generation patterns closely dependent on the aforementioned parameters. These parameters are primarily related to the coupling of the laser lightwave to the resonator (coupling ratio, offset of the laser lightwave with respect to the resonance, Q_{opt}, etc.) and to the specific characteristics of the resonator itself: material dispersion, geometric dispersion, laser lightwave wavelength, pumped optical mode family, Q_{opt-i}, FSR, intracavity power, etc. [23,44]. In order to further understand the complex dynamics of Kerr combs, different comb patterns (regimes) generated in the same optical mode in our MgF$_2$ WGMR (the identified useful optical mode) were studied and accurately characterized in the optical and the RF domains. We have particularly studied the relation between the blue offset of the laser lightwave with respect to the optical mode center and the generation of different comb patterns.

3.1. The various patterns of Kerr combs (blue slope of the pumped mode)

The experimental setup that we used to characterize the different Kerr comb patterns generated in the MgF$_2$ WGMR is depicted in Fig. 2(c). In this setup, the laser power at the input microfiber was set to 20 dBm and a polarization controller has been used before the WGMR in order to
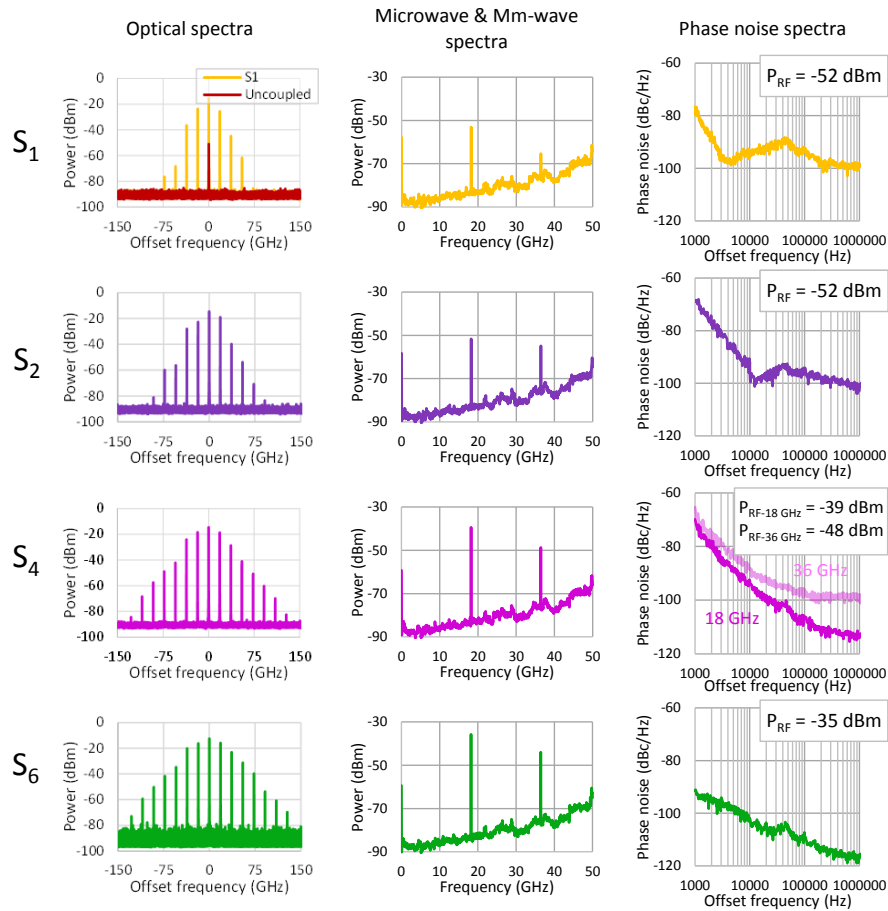
Fig. 4. Measured optical spectra at the drop port of the WGMR and their corresponding RF spectra, obtained for different Kerr comb patterns generated at different laser-mode locking states (see Fig. 3). The measured single sideband phase noise spectra of the Kerr combs' beat note at 18 GHz are given for locking states S_1, S_2, S_4 and S_6 with the corresponding carrier RF power. For state S_4, the phase noise spectra of both beat notes at 18 GHz and 36 GHz are given and compared. (OSA: RBW = 12.5 MHz; ESA: RBW = 50 kHz and VBW = 50 kHz).

optimize the WGMs excitation. Afterwards, the blue slope of the identified optical mode was probed. This was accomplished using the side-of-fringe laser locking technique as it allows accurate probing of the optical mode slope. In this locking scheme, when the laser lightwave is at the slope of the optical mode, the resonator absorption signal (or transmission signal) translates the partially-resonant laser frequency changes into intensity changes. These intensity changes are then fed back to the laser through a proportional-integral-derivative controller (PID) to stabilize it on the required mode slope. In order to reduce the noise in this laser-mode locking scheme, only the blue edge of the optical mode was investigated. This is due to the fact that the mode thermal drift in the MgF$_2$ WGMR has the same direction as the scanning lightwave if the lightwave is scanning the optical mode from its blue side towards its red side. Here, we should mention that no WGMR temperature stabilization setup was used.

The two optical outputs of the WGMR (add and drop ports) were each sent to an optical fiber coupler to be then split and sent simultaneously to an optical spectrum analyzer (OSA; APEX 2440B) and a fast photodiode (50 GHz u2t photodiode) followed by an electrical signal and spectrum analyzer (ESSA; Rohde & Schwarz FSW50) to be characterized. Before being split, the optical signal at the through port was attenuated using a variable optical attenuator (VOA) in order to protect the used instruments and components from the high laser power. Also, 10% of the through port signal were sent to a slow photodiode followed by an oscilloscope in order to monitor and control the laser-mode locking state. Here we should also mention that the drop port microfiber was only weakly coupled to the WGMR to couple out the optical signal from the WGMR. Various patterns of Kerr combs were generated and identified while the laser was gradually resonant in the identified optical mode of the MgF_2 WGMR. The translation from one pattern to another depended on the laser-mode locking state [see the inset figure in Fig. 3] because all the other experimental parameters were fixed. These states were then recorded and each related Kerr comb pattern was accurately characterized in the optical and the RF domains.

The measured optical spectra at the drop port of the WGMR and their corresponding RF spectra are depicted in Fig. 4 for the different identified Kerr comb patterns. These results show first the different generated Kerr comb patterns in the optical domain. As it can be seen, primary Kerr combs are generated in states S_1, S_2, S_4 and S_6. In the first three states, the generated narrow Kerr combs let us suggest that a hyper-parametric oscillation process is generated in the WGMR which features a small anomalous group velocity dispersion, like it has been reported in [23]. Indeed, the beat notes for the different Kerr combs featured relatively stable RF power, which is in agreement with the energy conservation process during the generation of Kerr combs.

It should be recalled that primary combs emerge through modulational instability when the WGMR is pumped above a certain threshold [19, 22]. They correspond to a roll pattern for the intracavity field, and feature a multiple FSR spacing in the frequency domain [45, 46]. This multiplicity can vary in significant proportions (from 2 to more than 200, see ref. [38]) and critically depends on the value of group-velocity dispersion (which can eventually be engineered, even for crystalline resonators [47]). However, the amplitude of these combs can not be set at arbitrarily high value by increasing the pump power, as this procedure unavoidably leads to the destabilization of the roll patterns, and to spatiotemporal chaos [48, 49].

Owing to the very good dynamic of the ESSA used in the experiment, we were able to measure the phase noise spectra of the central beat notes of the comb patterns generated at locking states S_1, S_2, S_4 and S_6. The measured single sideband phase noise spectra of the patterns for the beat note at 18 GHz are given with the corresponding carrier RF power (see Fig. 4). For state S_4, the phase noise spectra of both beat notes at 18 GHz and 36 GHz are given and compared, where a relatively similar close-in phase noise levels can be noticed. This confirms the generation of a coherent comb at this laser-mode locking state with correlated comb teeth. On the other hand, the higher noise floor obtained for the 36 GHz beat note is due to the lower RF power of the beat note.

For state S_6, where a noticeably very stable Kerr comb was generated, the measured phase noise spectrum for the carrier at 18 GHz gives phase noise levels of -92 dBc/Hz and -103 dBc/Hz at 1 and 10 kHz offset frequencies from the carrier, respectively. The measured RF power was also the highest among the other Kerr combs' beat notes at 18 GHz. For states S_3 and S_5, the combs were unstable and also the corresponding beat notes. This prevented their characterization in terms of phase noise in the RF domain. Moreover, we have investigated on the noise bump generated at 50 kHz offset frequency from the carriers in all the recorded phase noise spectra for all the comb patterns but without being able to identify its source. This noise bump could be due to the laser side-of-fringe locking scheme or even to another generated nonlinear optical effect like the Rayleigh scattering effect, whose gain could be centered at 60 kHz from an optical lightwave. This noise is later down-converted to the RF domain by the fast photodiode.
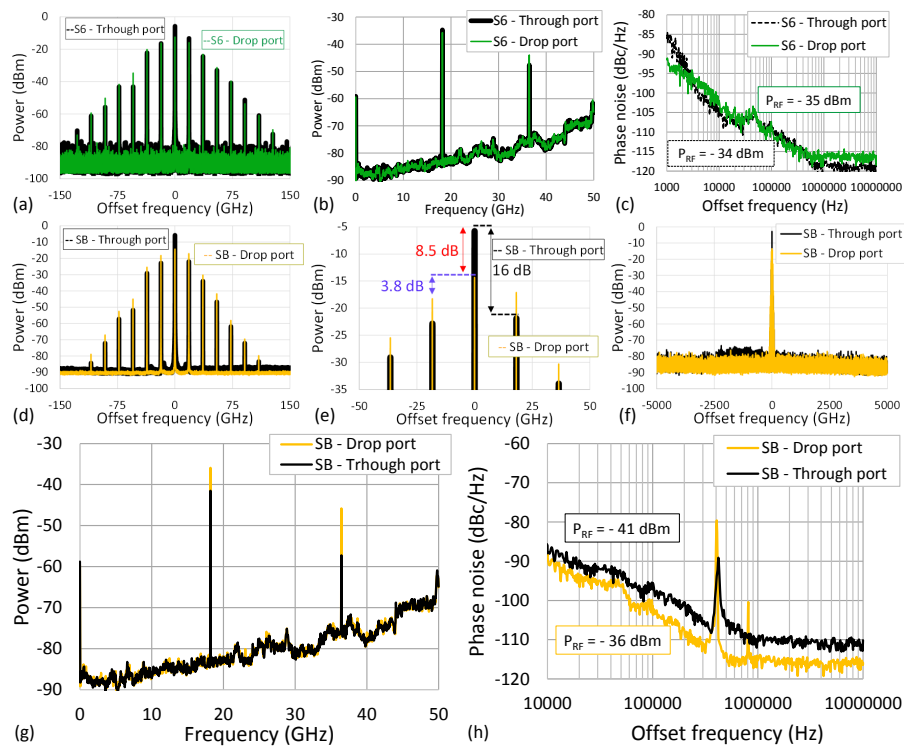
Fig. 5. Comparison of the comb performances at the through and drop ports of the WGMR. (a) Optical spectra, (b) RF spectra and (c) phase noise spectra recorded for a laser-mode locking state S_6. (d) Optical spectra, (e) narrow span optical spectra, (g) RF spectra and (h) phase noise spectra, recorded for a laser-mode locking state S_B (see the inset figure in Fig. 3). (f) A wide span (10 THz; 80 nm) optical spectra recorded for the laser-mode locking state S_B. OSA: RBW = 12.5 MHz [averaging = 100 for (d) and (e)]; ESA: RBW = 50 kHz and VBW = 50 kHz.

Despite the obtained low RF power levels, which are particularly due to the slightly coupled output optical signal at the drop port of the WGMR, these phase noise results are very encouraging. In addition, one has to take into consideration the laser locking on the slope of the optical mode, which greatly contributes to the conversion of any laser frequency noise into amplitude noise, thus degrading the performances of the generated beat notes in the RF domain. On the other hand, this experiment shows that even if the different Kerr comb patterns were generated in the same WGMR, in the same optical mode and in the same experimental conditions (except for the laser lightwave offset with respect to the optical mode), they enabled the generation of different microwave and millimeter-wave signals featuring clearly different performances [32].

3.2. *Performances at the through and drop ports*

To further investigate on the performances of the microwave and millimeter wave signals generated by the different comb patterns, we have measured and compared the optical, RF and phase noise spectra for the comb generated at the locking state S_6, simultaneously at the through and drop ports of the WGMR. The results are depicted in Figs. 5(a)–5(c). The optical spectra in Fig. 5(a) show a lower laser power at the drop port with a lower power gap between the laser lightwave and the neighboring comb teeth, contrarily to the optical spectrum obtained at
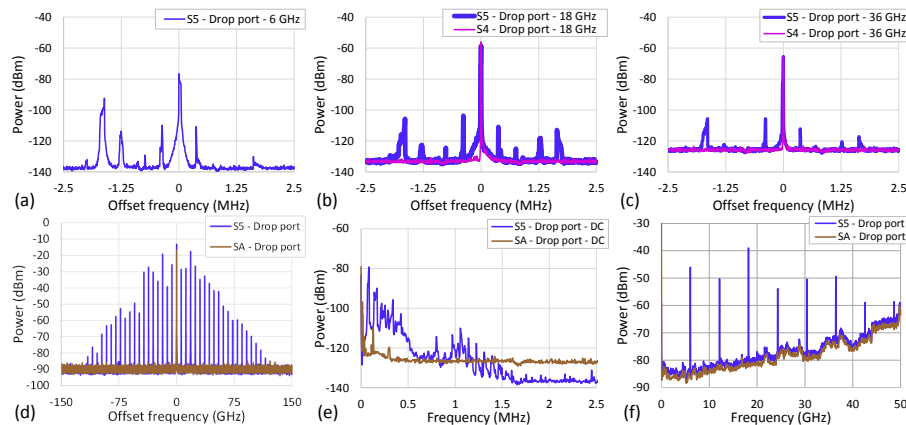
Fig. 6. Comparison of the Kerr comb performances at the WGMR drop port between states S_4 and S_5 [see the inset figure in Fig. 3 and Fig. 4]. (a), (b) and (c): RF spectra recorded for states S_4 and S_5 and centered at beat notes 6 GHz (only for S_5), 18 GHz and 36 GHz, respectively. (d) Optical spectrum, (e) low frequency DC spectrum and (f) Large span RF spectrum recorded for the Kerr comb generated at states S_5 and compared with state SA spectra where the laser lightwave was slightly resonant but no Kerr comb was generated [see the inset figure in Fig. 3].

the through port. On the other hand, a slightly lower RF power is obtained for the beat note at 18 GHz at the drop port [see Fig. 5(b)]. As expected, a better close-in phase noise level is obtained for the 18 GHz beat note at the drop port but with a higher noise floor due to a slightly lower RF power of the carrier.

Later on, the results provided in Figs. 5(a)–5(c), and suggesting better performances for the Kerr comb at the drop port, have been further confirmed by using another laser-mode locking state S_B [see the inset figure in Fig. 3]. The optical spectra, narrow span optical spectra, RF spectra and phase noise spectra, recorded for the Kerr comb pattern generated at state S_B are depicted in Figs. 5(d), 5(e), 5(g), 5(h). They give indeed further confirmation of logically better performances of the Kerr comb at the drop port of the WGMR. In the results presented in Figs. 5(d) and 5(e), where an averaging factor of 100 has been used, we can see that the laser lightwave was better rejected at the drop port and a much lower power gap between the laser lightwave and the neighboring comb teeth was also obtained (only 3.8 dB power gap between the laser lightwave and the first neighboring comb teeth for the drop port signal, compared to 16 dB gap for the through port signal). Here, one has to take into account the fact that in Figs. 5(a), 5(d), and 5(e), the lower optical power of the combs teeth at the drop port is due to the laser-WGMR under-coupling regime.

Correspondingly, higher RF power and lower phase noise levels are obtained for the 18 GHz beat note at the drop port. This is due to a lower power laser lightwave, preventing an early saturation of the photodiode and therefore leading to higher RF power levels and lower phase noise levels for the generated microwave and millimeter-wave beat notes (unlike the through port case where the photodiode is rapidly saturated by the high power laser lightwave). Here it is noteworthy to mention that higher optical and RF power levels could have been obtained at the drop port if the optical fiber coupler was not used (3 dB additional optical loss added by the optical fiber coupler in our experiment which can be equivalent to 6 dB additional loss in the RF domain if a quadrature detection of the photodetector is considered).

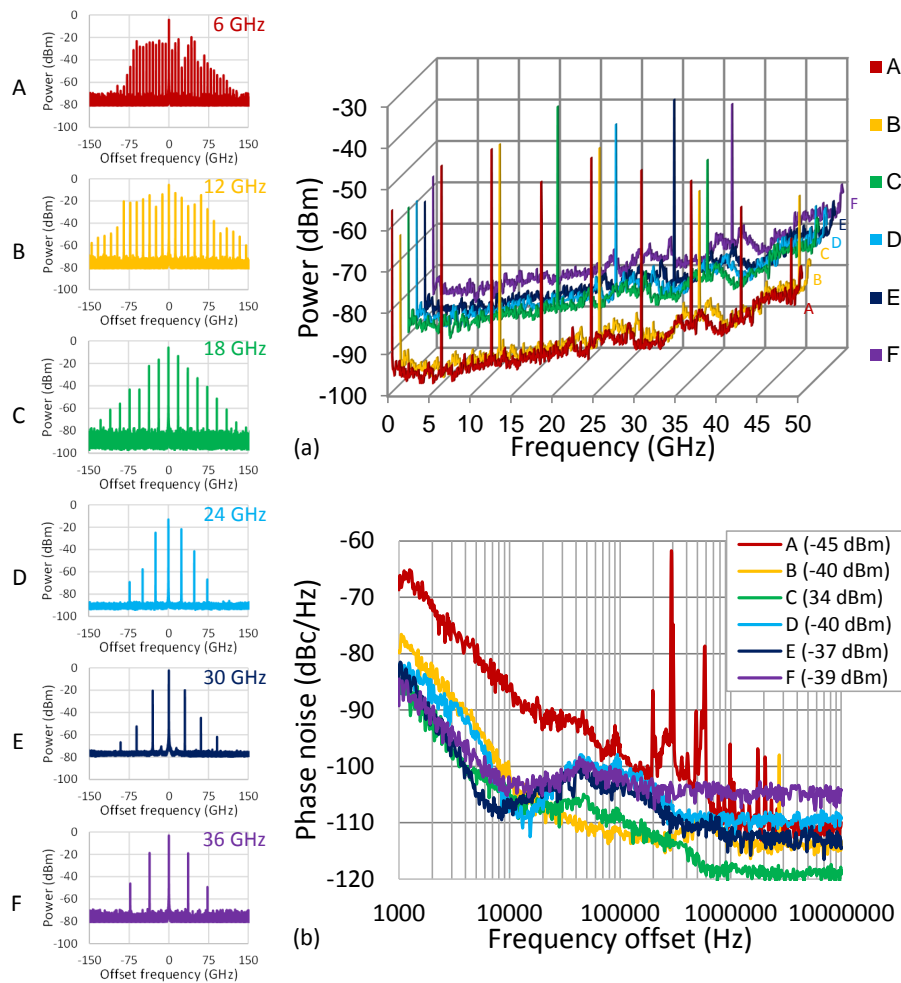All these results prove that one way to improve the conversion process of the generated Kerr

Fig. 7. Comparison of the performances of different Kerr combs (A–F) generated at the through port using different optical modes of the MgF$_2$ WGMR. (A–F) represent the optical spectra for the different combs. (a) Comparison of the wide span RF spectra of the different combs. (b) Comparison of the phase noise spectra of the main beat notes (i.e. 6–36 GHz, for the spectra A–F, respectively).

combs from the optical domain to the RF frequency domain is the use of the drop port instead of the through port. As a result, the photodiode will no longer be saturated by a high power laser lightwave. Additionally, the use of the drop port provides a noise filtering effect to the generated combs thanks to the high Q_{opt} of the WGMR. Finally, wide span (10 THz; 80 nm) optical spectra were recorded for state S$_B$ at the through and drop ports [see Fig. 5(f)]. This result proves well that a purely primary Kerr comb was generated for the laser-mode locking state S$_B$. Here, no verification of a possible existence of stimulated Raman scattering competing with the generated Kerr comb has been performed. This is due to the limited bandwidth of the OSA we used. However, nothing indicated the presence of such competition in our case.

3.3. Noisy Patterns

The overall noise present in the WGMR or generated by the pump process will have a critical influence on the spectral purity and coherence of the output comb [50, 51]. These stochastic fluctuations generate noisy Kerr comb patterns which have been investigated thoroughly in this work. We have especially characterized the comb generated at state S_5 at the drop port. Since the generated comb was a combination of primary and secondary combs, the beat of the comb on the fast photodiode gave rise to several beat notes in the RF domain. The recorded RF spectra at the ESSA, centered at the different generated microwave and millimeter wave signals, revealed the generation of excess noise peaks from either side of these signals. From the recorded RF spectra, centered at beat notes 6 GHz, 18 GHz and 36 GHz and presented in Figs. 6(a)–6(c), we can clearly notice that the excess noise peaks are the same for all the generated microwave and millimeter wave signals (same observation for the other beat notes at 12 GHz, 24 GHz, 30 GHz, 42 GHz and 48 GHz). Those spectra were also compared to the RF spectra recorded for state S_4 at 18 GHz and 36 GHz, where pure RF spectra were obtained with no sign of any excess noise peaks [see Figs. 6(b)and 6(c)]. This is because the generated Kerr comb in state S_4 was a coherent primary comb.

At state S_A, the laser lightwave was slightly resonant but no comb was generated [see the inset figure in Fig. 3 and Fig. 6(d)]. Therefore, any excess noise peaks generated at state S_A will be caused by the laser frequency noise itself, converted into amplitude noise through the laser-mode side-of-fringe locking scheme as it has been demonstrated in [52]. As part of our further investigations performed to determine the origin of the parasitic noise peaks, we have recorded and compared the optical spectrum, low frequency DC spectrum and large span RF spectrum for the Kerr comb generated at states S_5 and compared them with the spectra recorded at state S_A [see Figs. 6(d)–6(f)]. The obtained experimental results, and particularly the recorded low frequency DC spectra in [Fig. 6(e)], allowed us to exclude a relation between a laser converted noise and the generated excess noise peaks. Subsequently, the excess noise peaks observed at state S_5 (and also at state S_3) are most probably due to bad overlaps between the different adjacent non-phase-locked secondary combs (featuring a 6 GHz FSR_c), generated each around a tooth of the primary comb (featuring an 18 GHz FSR_c) [23, 24]. These bad overlaps are then detected as beat notes after the photodiode, thus generating excess noise peaks around the main beat notes (6 GHz, 12 GHz, etc.).

Aside from that, the thermal noise is another noise type that should be taken into account while using Kerr generated combs in a WGMR to later generate low noise microwave and millimeter wave signals. Indeed, as the laser is scanning through the optical mode of the MgF_2 WGMR, the heat generated by the gradually resonant lightwave progressively expands the resonator diameter and therefore reduces its FSR. As a result, the generated comb beat notes' frequency is also reduced (6 GHz, 12 GHz, 18 GHz, etc.). Contrariwise, a less resonant laser will reduce the generated heat in the resonator and the beat notes' frequency will consequently increase. As a result, any laser frequency noise will be also "thermally" converted into frequency noise of the generated RF beat notes. The efficiency of this noise conversion phenomenon will particularly depend on the coefficient of thermal expansion of the resonator bulk material.

3.4. Phase noise of microwave and millimeter-wave beatnote signal

The different optical modes used for comb generation featured closely similar performances (FSR and Q_{opt}) and were all excited by the same Koheras laser used in the previous experiments. The experimental setup is the same as the one depicted in Fig. 2(c). Moreover, an optical power level of 20 dBm was used at the input microfiber. On the other hand, a specific locking state was used for each generated comb. The optical spectra of the different generated combs are depicted in Figs. 7(a)–7(f). As we can see from these spectra, both combs in both (A) and (B) are not pure primary combs. The intermodal frequency is equal to 6 GHz in (A) and to 12 GHz in (B).

However, for (C), (D), (E), and (F), the spectra indicate that the generated combs are genuinely primary.

The wide span RF spectra of the beat note of the aforementioned combs on a fast photodiode were recorded and are presented in Fig. 7(a). Likewise, the phase noise spectra of the main signal generated by each comb (i.e. the signal with a frequency equal to the comb intermodal frequency) have been recorded. The measured phase noise spectra are presented in Fig. 7(b) along with the obtained RF power for the generated signals. These phase noise results well confirm our assumption on better performances for purely primary combs. For signals generated by combs (C)(D)(E) and (F), phase noise levels below -100 dBc/Hz at 10 kHz offset frequency from the different carriers have been obtained. It is also clear that the microwave signal generated at 6 GHz by the Kerr comb in (A) features the worst phase noise and RF power results compared to the other generated microwave and millimeter-wave signals. The microwave signal generated at 12 GHz has better performances than the 6 GHz signal but inferior performances compared the other remaining signals. This further proves that, in combs formed from a combination of primary and secondary combs, the more teeth are involved, the worse secondary comb overlaps are obtained, which finally results in a noisy comb beat note in the RF domain. Of course, at certain conditions, a phase locking can occur for the different generated secondary combs in such comb regimes. This is obtained when FSR_c of the primary comb is nearly an integer multiple of the FSR_c of the secondary combs. Still, purely primary comb patterns seem to be however safe patterns to generate low phase noise microwave and millimeter-wave signals.

4.   Conclusion

In this article we presented several investigations performed on Kerr optical frequency combs generated in a high quality factor whispering gallery mode optical resonator made of magnesium fluoride. The investigations were focused on the identification of different comb patterns generated in the same optical mode of the WGMR in function of the pumping laser lightwave offset from the optical mode center. This has been achieved by using the side-of-fringe laser locking technique in order to accurately probe the blue slope of the optical mode. Various comb patterns were identified and the performances of the corresponding microwave and millimeter-wave signals, generated by beating those patterns on a fast photodiode, have been characterized in terms of power and phase noise in the RF domain.

An even better understanding of Kerr comb formation can be achieved if our investigation method could be also performed on the red side of the optical mode. This could also provide a better understanding of solitons formation and performances, which are likely to be generated by a red detuned laser lightwave (with other specific conditions). Moreover, the study of Kerr comb formation when a laser locking at the center of the optical mode is achieved, could be of great interest as the generated comb properties would only depend on the power level of the pumping laser. Also, laser locking noise and noise conversion phenomena can be avoided in that case. All these complementary studies will certainly pave the way for fully controlled and efficient chip-scale devices based on Kerr combs, which will be the trigger for a new technological breakthrough. Further research will also focus on the role of other scattering phenomena [53,54] on the phase noise performance of these microwave photonic oscillators. In particular, specific efforts will be devoted to investigate coupling mechanisms that can guarantee improved stability and robustness against external vibrations and fluctuations.